Algal Research 98 (2026) 104852

Contents lists available at ScienceDirect

Algal Research

journal homepage: www.elsevier.com/locate/algal

Biophysical and structural characterization of biocompatible microalgae-derived vesicles as sustainable drug delivery platforms

Nadica Ivošević DeNardis [a,*], Tea Mišić Radić [a], Mária Klacsová [b], Daniela Uhríková [b], Ruža Frkanec [c], Joanna Zemła [d], Malgorzata Lekka [d], Martin Lukeš [e], Ondrej Prášil [e], Krisztina Sebők-Nagy [f], Tibor Páli [f], Katarina Lisac [a], Marcela Chovancová [b], Karlo Ojdanić [g], Lucija Horvat [a], Petra Peharec Štefanić [g], Kristina Smoković [a], Nadica Maltar-Strmečki [a], Dijana Pavlović Saftić [a], Ivo Piantanida [a], Tanja Matijević Glavan [a]

[a] Ruđer Bošković Institute, Bijenička cesta 54, 10000, Zagreb, Croatia
[b] Faculty of Pharmacy, Comenius University Bratislava, Odbojárov 10, 83232, Bratislava, Slovakia
[c] Centre for Research and Knowledge Transfer in Biotechnology, University of Zagreb, Rockefellerova 10, 10000, Zagreb, Croatia
[d] Institute of Nuclear Physics Polish Academy of Sciences, ul. Radzikowskiego 152, 31-342, Kraków, Poland
[e] Institute of Microbiology of the Czech Academy of Science, Centre of Algatech, Novohradská 237 - Opatovický mlýn, 379 01, Třebon, Czech Republic
[f] Institute of Biophysics, HUN-REN Biological Research Centre, Temesvári krt. 62, 6726 Szeged, Hungary
[g] Faculty of Science, University of Zagreb, Horvatovac 102a, 10000, Zagreb, Croatia

ARTICLE INFO

Keywords:
Biocompatibility
Drug delivery
Ghost vesicles
Membrane structure
Cargo binding
Microalgae-derived vesicles
Self-assembly

ABSTRACT

Marine microalgae are sustainable sources of bioactive compounds and drug delivery platforms that can utilize whole cells, cell fragments, or vesicles. Although extracellular vesicles secreted by microalgae have shown potential, broader application is limited by low yields, instability, complex isolation, and poor standardization. To address these challenges, we previously proposed an alternative strategy in which hypoosmotic stress induces cell disruption, followed by self-assembly of membrane fragments into reconstructed microalgae-derived vesicles. Here, a comprehensive biophysical approach combining top-down and bottom-up strategies provides insight into vesicle structural features relevant to their function as drug delivery platforms. They form a heterogeneous population but can be reduced to the nanometer range. Their pigmented membranes contain chlorophyll degradation products and carotenoids, and provide significant antioxidant activity. The protein-to-lipid ratio of cells and vesicles is maintained mainly during self-assembly, indicating an effective reconstruction process. Vesicles have a balanced fatty acid profile, hydrophilicity, pronounced softness, and structure-dependent permeability. *In vitro* cytotoxicity studies indicated that vesicles do not exhibit acute cellular toxicity and show only mild, cell line-dependent effects at high concentrations. An *in vivo* immunogenicity study also demonstrated mild adjuvant activity. Confocal imaging shows that a glycopeptide antibiotic and an oligonucleotide bind via non-covalent interactions with the membrane surface. A lyophilization and rehydration protocol was developed to extend material stability, highlighting the importance of the self-assembly process during which vesicle morphology is preserved. These findings provide proof of concept that reconstructed microalgae-derived vesicles can be used to develop next-generation sustainable and safe drug delivery platforms.

1. Introduction

Sustainable, environmentally friendly materials such as marine microalgae are in high demand in biotechnology for their antioxidant, antibacterial, antiviral, and neuroprotective properties. Marine microalgae produce a wide range of biorefinery products, including biofuels, food supplements, and natural dyes, which have applications in healthcare (anti-aging therapies, cancer treatment), agriculture (biofertilizers), and environmental management (wastewater treatment) [1–7]. Despite the many established applications, microalgae-based

* Corresponding author at: Ruđer Bošković Institute, Bijenička cesta 54, 10000, Zagreb, Croatia.
E-mail address: ivosevic@irb.hr (N. Ivošević DeNardis).

https://doi.org/10.1016/j.algal.2026.104852
Received 6 December 2025; Received in revised form 22 May 2026; Accepted 17 July 2026
Available online 20 July 2026

materials have attracted increasing interest as delivery systems over the past decade. Several approaches have been developed for microalgae-based delivery systems, including intact algal cells, cell fragments, extracellular vesicles (EVs), and reconstructed membrane vesicles. For example, antibiotics have been transported by chemically modified green microalgae [8], and ibuprofen has been delivered using hollow microspheres produced from microalgae by spray pyrolysis [9]. Diatom shells coated with biosilicate have shown promise for drug and gene delivery in cancer treatment [10,11]. The pronounced motility of microalgae, combined with magnetic fields, has enabled precise drug delivery [12]. In addition to intact cells, cell wall constituents have been incorporated into microgels for antigen delivery [13]. Furthermore, microalgae-derived vesicles can be generated in two ways. First, EVs released by microalgal cells in healthy or pathological states have been shown to be biocompatible, exhibit low heterogeneity, and can serve as nanocarriers for bioactive substances. However, low yield, lack of standardization, and limitations in stability, loading, and targeted delivery, as well as the need for costly and complex isolation methods, still need to be addressed [14,15].

Second, reconstructed microalgae-derived vesicles are formed by self-assembly of fragmented cell membranes through non-covalent interactions [16–18]. The microalga *Dunaliella tertiolecta* is common in aquatic ecosystems and shows significant adaptability to fluctuating salinity levels, making it a suitable candidate for this application. This species is known as a naked cell, as its soft, semi-permeable plasma membrane with a glycocalyx surface coating supports its use in osmoregulation studies [7]. The reconstructed microalgae-derived vesicles constitute a complex, multicomponent physicochemical system, and current understanding of these vesicles remains limited. To address this, we used a comprehensive biophysical approach combining top-down and bottom-up strategies to provide insight into vesicle structural features relevant to potential drug-delivery applications. A variety of imaging techniques, such as Atomic Force Microscopy (AFM), Transmission Electron Microscopy (TEM), Confocal Laser Scanning Microscopy (CLSM), and fluorescence microscopy were used to characterize the size, shape, and thickness of the vesicles as well as their mechanical and chemical properties and drug transportability. In addition, bulk techniques such as Spectrophotometry to assess biocompatibility, Electron Paramagnetic Resonance (EPR) for membrane function, and advanced analytical methods (Gas Chromatography Flame Ionization Detector (GC-FID), High Performance Liquid Chromatography (HPLC), Fourier Transform Infrared Spectroscopy (FTIR) were used to characterize the composition of cells and vesicles. This study could support the development of sustainable microalgae-derived vesicles for next-generation delivery technology.

2. Materials and methods

2.1. Cell culture

The unicellular marine microalga *Dunaliella tertiolecta* Butcher (DT, Chlorophyceae, CCMP 1320, Culture Collection Bigelow Laboratory for Ocean Sciences, Bigelow, MN, USA, with a length of 6–12 μm) was cultured in natural seawater in Erlenmeyer flasks. In brief, the F-2 medium was prepared using natural seawater from the Adriatic Sea [19]. After preparing the growth medium, a cell aliquot was added to achieve an initial monoculture density of approximately 4×10^4 cells mL^{-1}. Flasks were sealed with sterile cotton plugs to prevent contamination, and cells were cultured under ambient conditions (18 °C, constant shaking at 20 rpm, 12 h light:12 h dark cycle with an irradiance of 31 μmol photons m^{-2} s^{-1}). The average cell number was determined from triplicate samples using a Fuchs-Rosenthal haemocytometer (Fein-Optik Jena, Germany, with a depth of 0.2 mm) and a light microscope (Olympus BX51, Olympus Corporation, Japan) at 40 × magnification. After 12 days of growth, the cells reached the early stationary growth phase, and the cell density was between 2 and 6×10^6 cells mL^{-1}. The cells were isolated from the growth medium by gentle centrifugation (1500 ×*g*, 5 min, HICEN21, Herolab GmbH, Wiesloch, Germany), followed by repeated rinsing with filtered seawater.

2.2. Preparation of reconstructed microalgae-derived vesicles from the cell suspension

The hypoosmotic shock of photosynthetic marine microalgae DT resulted in the formation of reconstructed microalgae-derived vesicles (known as ghost vesicles, GVs), as previously described [17,18]. In brief, microalgae were isolated from the growth medium at early stationary phase by centrifugation, and 4 mL of the loose cell pellet was diluted 40-fold with ultrapure water (Milli-Q, Merck Millipore, Billerica, MA, USA), vortexed vigorously, and left at room temperature for 30 min to allow osmotic shock. Within 1 min, a dramatic change in cell shape occurs, with some cells becoming deformed and showing an initial loss of intracellular content. After 10 min, there are no cells left. The resulting mixture contains partially or completely empty vesicles as well as clumps of free-flowing debris. To obtain the purest possible suspension of empty GVs, the following purification procedures were performed. The sample was centrifuged (HICEN21, Herolab GmbH, Wiesloch, Germany) at 2000 ×*g* for 5 min at 18 °C. The pellet and supernatant were then examined under a light microscope. The pellet contained a large amount of released intracellular material, both non-empty and empty vesicles. The supernatant was centrifuged at 7500 ×*g* for 12 min at 18 °C to remove residual material and free-floating debris. After centrifugation, the pellet contained mainly debris and some vesicles, but the supernatant contained mainly reconstructed empty vesicles and vesicles with residual material concentrated in a thin, viscous layer adjacent to the pellet. The concentration of reconstructed microalgae-derived vesicles in the aqueous suspension (pH 6.68) was between 10^4 and 10^6 vesicles mL^{-1}, with diameters of up to 30 μm. For the cytotoxicity study, the vesicle suspension was briefly sonicated with an ultrasonic probe (diameter 1 mm, amplitude 50% of nominal power, duration 30 s, Labsonic M, B. Braun Biotech International/Sartorius Group, Göttingen, Germany). The primary GV suspension was used for chemical profiling (FTIR), mechanical and chemical measurements (AFM force spectroscopy), antioxidant activity (EPR), cytotoxicity, immunogenicity assays, and cargo–membrane association experiments.

2.3. Preparation of reconstructed microalgae-derived vesicles from lyophilized material

An additional protocol was developed for the reconstruction of vesicle samples by hydration of lyophilized material (post-processed vesicle samples). The suspension of reconstructed vesicles (as described in section 2.2) was stored overnight at −20 °C and then lyophilized for 24 h (−50 °C, 10 Pa, Freezone 2,5; Labconco, Kansas City, MO, USA). The lyophilized material was hydrated to achieve a concentration of 1 mg mL^{-1}. The suspension was homogenized by repeated vigorous vortex mixing and gentle intermittent sonication in a bath (K5LE, Kraintek, Czech Republic) and then stored at 4 °C. During the 48-h storage period, the sample was vortexed 6 times for 20–30 s each. The vesicle suspension was then extruded in 21 passes through a polycarbonate filter with a pore size of 200 nm (Whatman, Nucleopore, Cytiva, Marlborough, MA, USA) using a Liposofast Basic extruder (Avestin, Ottawa, Canada) with two gas-tight syringes (Hamilton, Reno, NV, USA) at room temperature (MacDonald et al. 1991). An odd number of passes was performed to avoid contamination by vesicles that might not have passed through the filter. These post-processed vesicle samples were subjected to AFM imaging in air and liquid.

2.4. Model drugs

Table 1 summarizes the physicochemical properties and applications of the selected model drugs.

Table 1
Physicochemical properties and application of selected model drugs: vancomycin-FITC, and oligo-DNA-FAM.

Properties and application	Model drugs	
	vancomycin-FITC	oligo-DNA-FAM
Chemical formula	$C_{87}H_{88}Cl_2N_{10}O_{29}S$	–
Molecular mass	1840 g mol^{-1}	7834.2 g mol^{-1}
$\lambda_{ex.}$/nm	498	495
$\lambda_{em.}$/nm	517	520
Solubility	–	1 mg mL^{-1}
Log *Po/w*	−0.71[a]	–
Application	Antibiotic	Gene therapy

[a] Spectrophotometrically determined in this study.

The vancomycin-FITC was purchased from Sigma-Aldrich (St. Louis, Missouri, United States). The model DNA used in this study (purchased from an IDT Technologies® certified supplier, Coralville, Iowa, United States) was a 12-mer GC-duplex homopolymer labeled with fluorescein (FAM) at the 5′ end. The fluorophore is connected to the oligonucleotide sequence via a six-methylene long linker, which prevents intramolecular fluorescence quenching and ensures an optimal spectroscopic response. The stock solution for vancomycin-FITC in aqueous form was 5×10^{-5} M, while the stock solution for oligo-DNA-FAM in Tris buffer was 1×10^{-3} M. Both fluorophores (FITC and FAM) were selected so that their emission wavelengths did not overlap with the autofluorescence of the vesicles and were complementary to the lipophilic dye DiI, which was used to stain the membranes.

2.5. Optical and fluorescence imaging and sample preparation

An Olympus BX51 fluorescence microscope (Olympus, Tokyo, Japan) was used to determine cell and vesicle densities. Confocal measurements were performed using a Leica TCS SP8 confocal laser scanning microscope (CLSM, Leica, Wetzlar, Germany) with a white-light laser and a 63× (N.A. = 1.4) oil-immersion objective to investigate drug transportability. The slides were cleaned with ethanol, rinsed several times with water, and dried with a stream of nitrogen.

Subsequently, 50 μL of polyethylenimine (PEI; Sigma-Aldrich Corporation, St. Louis, MO, USA) was added to the slide and incubated for 30 min; the PEI drops were then removed. 20 μL of an aliquot of the vesicles was added to the modified slide and incubated for 30 min.

A final concentration of 2 μM of DiI fluorescent dye (Sigma-Aldrich Corporation, St. Louis, MO, USA) was added prior to imaging. Then 1 μL of 1×10^{-5} M DNA-FAM and 5×10^{-5} M vancomycin-FITC were added. The spectral settings for the two selected model drugs were the same: excitation line 495 nm and emission range 505–550 nm. To better visualize the vesicles, the lipophilic membrane dye DiI (excitation maximum 552 nm, emission range 570–600 nm) was used. The concentration of the stock solution of the dye DiI prepared in DMSO was 2×10^{-4} M.

2.6. Composition of reconstructed microalgae-derived vesicles and microalgal cells

The macromolecular compositions of the vesicle and cell suspensions were determined by FTIR spectroscopy in transmission mode, as described in a previous study [20] and briefly in the supplementary material.

2.7. Lipids, fatty acids, and pigments: extraction and analysis

Lipids were extracted with dichloromethane, methanol and water as described in previous study [21]. Separation of lipid classes was performed using thin-layer chromatography. Quantitative and qualitative analysis of fatty acids was performed using gas chromatography after direct esterification of the isolated vesicles. The method for sample preparation and analysis is described in [22] and the supplementary material. The pigments were extracted with water: methyl tert-butyl ether (MTBE) (1:1 *v*/v) by sonication and disruption with 0.1 mm zirconia beads. After crushing and extraction, samples were centrifuged at 7500 ×*g* for 10 min to achieve phase separation. The upper phase was transferred to a fresh vial. An aliquot of 500 μL MTBE was added, and the material was re-extracted until the interphase layer was white. The extracted pigments were evaporated in a SpeedVac (Thermo Scientific, Waltham, MA, USA) and diluted to 100 μL in MeOH. The pigments were analyzed by HPLC (Agilent 1260 series with equipped DAD and FL modules; Agilent, Santa Clara, CA, USA) and separated on a reversed-phase column (Zorbax Eclipse plus C18, 3.5 μm particle size, 4.6 × 100 mm; Agilent, Santa Clara, CA, USA). The extract was loaded with 35% methanol and 15% acetonitrile in 0.25 M pyridine (solvent A), and the pigments were eluted with a linear gradient of solvent B (20% methanol, 20% acetone in acetonitrile; 60–100% gradient over 25 min), followed by 100% solvent B (flow rate 0.8 mL min^{-1}, 40 °C).

2.8. Sample preparation for TEM imaging

For visualization by TEM, GVs were first incubated on a Formvar®/carbon/copper grid for 3 min and washed in ultrapure water (Milli-Q, Merck Millipore, Billerica, MA, USA). The sample was then incubated with a UranyLess™ contrast staining solution (Em-Grade, Mauressac, France) for 3 min and washed three times in ultrapure water after staining. After drying the sample, the vesicles were visualized using a Morgagni 268D transmission electron microscope (FEI, Eindhoven, Netherlands) at 70 kV. The choice of the operating voltage was made in particular to improve the mass-thickness contrast, which is very convenient for imaging fragile biological structures such as vesicles. It should be noted that negative staining under these conditions tends to emphasize the periphery (the “halo” effect) rather than the internal ultrastructure of the vesicle.

2.9. Atomic force microscopy imaging and sample preparation

Imaging of GVs in air was performed using a Multimode Scanning Probe Microscope with Nanoscope IIIa controller (Bruker, Billerica, MA, USA) equipped with a 125 μm vertical engagement (JV) scanner. To prepare the sample for imaging in air, 5 μL of the post-processed vesicle sample was deposited on freshly cleaved mica. The samples were placed in closed Petri dishes for 45 min to dry, then imaged. The contact mode was performed with silicon nitride cantilevers (DNP, Bruker, nominal frequency of 18 kHz, nominal spring constant of 0.06 N m^{-1}, and the nominal tip radius of 20 nm). The linear scan rate was between 1.5 and 2 Hz with a scan resolution of 512 samples per line. To minimize the interaction forces between the tip and the surface, the setpoint was kept at the lowest possible value. The images were processed and analyzed using NanoScope Analysis Software (version 2.0, Bruker, Billerica, MA, USA) [23].

Imaging of the post-processed vesicle sample in liquid (ultrapure water) was performed using a JPK NanoWizard 4 XP coupled to an Olympus IX73 (Bruker, Billerica, MA, USA). A glass slide was coated with 0.1% polyethylenimine (PEI; Sigma-Aldrich, St. Louis, MO, USA) and ultrapure water served as the imaging buffer. An aliquot of 100 μL of the post-processed vesicle sample was pipetted onto the PEI-modified slide and incubated for 1 h to allow the vesicles to settle and adhere to the surface. The sample was rinsed three times with 100 μL ultrapure water to remove non-adherent vesicles. After the last rinse, 150 μL ultrapure water was added. Imaging was performed in quantitative imaging (QI) mode with silicon nitride probes (MLCT, Bruker, nominal frequency 7 kHz, spring constant 0.01 N m^{-1}) using the following settings: setpoint 0.5 nN, z-length 600 nm, z-speed 50 μm s^{-1} and 128-pix resolution. The data were processed with JPKSPM Data Processing Software 7.0.165 (Bruker, Berlin, Germany), [24].

2.10. Atomic force microscopy - based force spectroscopy

The mechanical and hydrophobic properties of the GVs were measured using an AFM (NanoWizard 4 XP, Bruker, Billerica, MA, USA) in force spectroscopy mode. The AFM was combined with an inverted optical microscope (IX73, Olympus, Japan), allowing real-time observation of the sample. The vesicles were probed with a soft (nominal spring constant of 0.01 N m^{-1}) triangular silicon nitride MLCT-C cantilever (Bruker, Germany) with a four-sided pyramidal tip. The probes were calibrated using the thermal noise method [25]. To determine the hydrophobic properties of the vesicles, force spectroscopy measurements were performed with hydrophilic (bare) and hydrophobically modified trichlorooctadecylsilane (OTS; Sigma-Aldrich Corporation, St. Louis, MO, USA) probes using chemical vapor deposition. The chemical modification of the probes followed the protocol from our previous work [26]. Twenty vesicles were analyzed with unmodified (no OTS) and modified (OTS) probes. Data were analyzed with JPK Data Processing Software version 8.0.103 (Bruker-JPK, Berlin, Germany) [27].

2.11. Determination of the apparent Young's modulus and hydrophobic properties of reconstructed microalgae-derived vesicles

The mechanical properties of reconstructed micrometer-sized algae-derived vesicles were evaluated by determining the apparent Young's modulus (E_{app}), which served as a comparative metric between empty and non-empty populations. E_{app} was extracted from the approach part of the force-distance curves fitted with the Hertz-Sneddon model [28]. Given the use of four-sided pyramid probe, the relationship between the loading force (F) and the indentation depth (δ) is:

$$F = \frac{E}{1-\mu^2}\frac{tan\alpha}{\sqrt{2}}\delta^2$$

where α is the face-angle of the probe, and μ is the Poisson's ratio, here 0.5 because we assume that the vesicles are an incompressible material. Curves were fitted up to an indentation depth of 2 μm. For micrometer-sized GVs in this study (average diameter ~ 12 μm), this indentation represents approximately 16% of the total height, ensuring the analysis remains outside the "bottom-effect" regime. We utilized this framework to provide a robust, comparative indicator of stiffness while avoiding systematic errors associated with estimating shell thickness or internal pressure in heterogeneous populations - a practice well-supported by recent literature [29].

The hydrophobic properties were extracted from the retraction part of the force-distance curve using the method described previously [26]. Briefly, we use the difference in maximum work of adhesion (ΔW_{adh}) between the hydrophilic (no OTS) and hydrophobic (OTS) probe and vesicles, W_{adh} (no OTS) and W_{adh} (OTS), respectively. The negative value of ΔW_{adh} indicates the hydrophobic properties of the vesicles. The W_{adh} data are given as mean ± SD.

2.12. EPR spectroscopy sample preparation and measurements

Spin label 2,2,6,6-tetramethylpiperidine-1-oxyl (TEMPO) (Sigma-Aldrich Corporation (St. Louis, MO, USA) was dissolved in ultrapure water (Synergy® Water Purification Systems, Merck Millipore KGaA, Darmstadt, Germany) to prepare a stock solution (1×10^{-2} M). L-ascorbic acid and hydrogen-peroxide were purchased from Merck, Budapest, Hungary.

Algae suspension (4×10^6 algal cells per tube for each sample) and rehydrated lyophilized ghost vesicles (1×10^6 GVs per tube for each sample) were evenly distributed into Eppendorf tubes. After centrifugation at 23180 ×g (Hettich EBA 12 R, Tuttlingen, Germany) for 30 min at 4 °C, the supernatant was discarded. The pellet was resuspended in 100 μL of water, incubated at 40 °C for 10 min and shaken three times. After incubation, 4 μL of TEMPO (1×10^{-2} M) was added and the sample was incubated at 40 °C for 10 min, shaken three times, then transferred to a capillary tube and centrifuged at 1500 ×g for 5 min at room temperature before the supernatant was removed. For the three types of control experiments, 4 μL of TEMPO (1×10^{-2} M) was added to 100 μL of water, 1×10^{-3} M ascorbic acid, and 1×10^{-3} M H_2O_2 solution. Four microliters of each control were transferred into the capillary tube for measurements. It should be noted that the above procedures unavoidably led to different lag times from the onset of the reaction to recording the signal decay: typically 2–3 min for the aqueous solutions and 20–25 min for the suspensions.

Continuous wave EPR measurements were conducted using a Bruker ELEXSYS-II E580 X-band spectrometer (Bruker BioSpin GmbH, Rheinstetten, Germany) at room temperature with the following instrument settings: scan range, 3300–3400 G; microwave frequency, approximately 9.42 GHz; microwave power, 9.464 mW; modulation frequency, 100 kHz; modulation amplitude, 0.5 G; field axis resolution, 1024; number of scans, 4; sweep time, 40.96 s. Temperature was controlled using a Bruker variable-temperature device (Bruker BioSpin GmbH, Rheinstetten, Germany) with a liquid/gas nitrogen flow. Data analysis, fitting, and visualization were conducted using Igor Pro, version 8.02 (Metrics, Lake Oswego, Oregon 97,035, USA), [30].

2.13. Cell lines and cytotoxicity assay

Human cancer cell lines (Detroit 562 (pharyngeal carcinoma), SW480 (primary colon carcinoma), SW620 (metastatic colon carcinoma), HCT116 (colon carcinoma), HEK293T (human embryonal kidney cells)) were maintained in Dulbecco's modified Eagle medium (Sigma-Aldrich, Schnelldorf, Germany) supplemented with 2×10^{-3} M glutamine, 10% fetal calf serum, 100 U mL^{-1} penicillin, and 100 μg mL^{-1} streptomycin in a humidified chamber at 37 °C and 5% CO_2. All cell lines were obtained from ATCC. Cell abundance and viability were determined using the Neubauer counting chamber and Trypan Blue exclusion.

The protein concentration of the vesicles was determined using the Bradford assay. The vesicles were diluted in the cell medium according to the results of the Bradford assay before the cells were treated. Cell proliferation was measured using the MTT Cell Proliferation Assay (Sigma-Aldrich, Schnelldorf, Germany). Absorbance was measured at 570 nm using a microplate reader, Multiskan RS-232C (Thermo Fisher Scientific Inc., Austria). Cells were plated at 5×10^3 cells per well in 96-well microplates (TPP, Trasadingen, Switzerland) and treated with 0.1, 0.5, and 2 μg mL^{-1} vesicles (protein content) for 72 h. Each test point was performed in triplicate in four individual experiments.

2.14. Immunogenicity analysis: reagents and materials

Bovine serum albumin, Tween 20, monoclonal anti-chicken egg albumin (clone OVA-14 mouse IgG1 isotype), *o*-phenylenediamine dihydrochloride were provided by Sigma-Aldrich, Schnelldorf, Germany. Horseradish peroxidase-conjugated goat anti-mouse IgG (HRP-anti-mouse IgG) was from Bio-Rad Laboratories (USA). Biotin-conjugated rat antimouse IgG1 and antimouse IgG2a monoclonal antibodies and streptavidin−peroxidase were from PharMingen, Becton Dickinson (USA). Chemicals for buffers and solutions were purchased from Kemika d.d. (Zagreb, Croatia). Ovalbumin was purchased from Serva Electrophoresis GmbH, Heidelberg, Germany. Details can be found in the supplementary material.

3. Results

3.1. Chemical characterization of microalgae-derived vesicles and cells

FTIR spectroscopy was used for qualitative and semi-quantitative analysis of the GVs and DTs (Fig. 1a). Comparison between DTs and

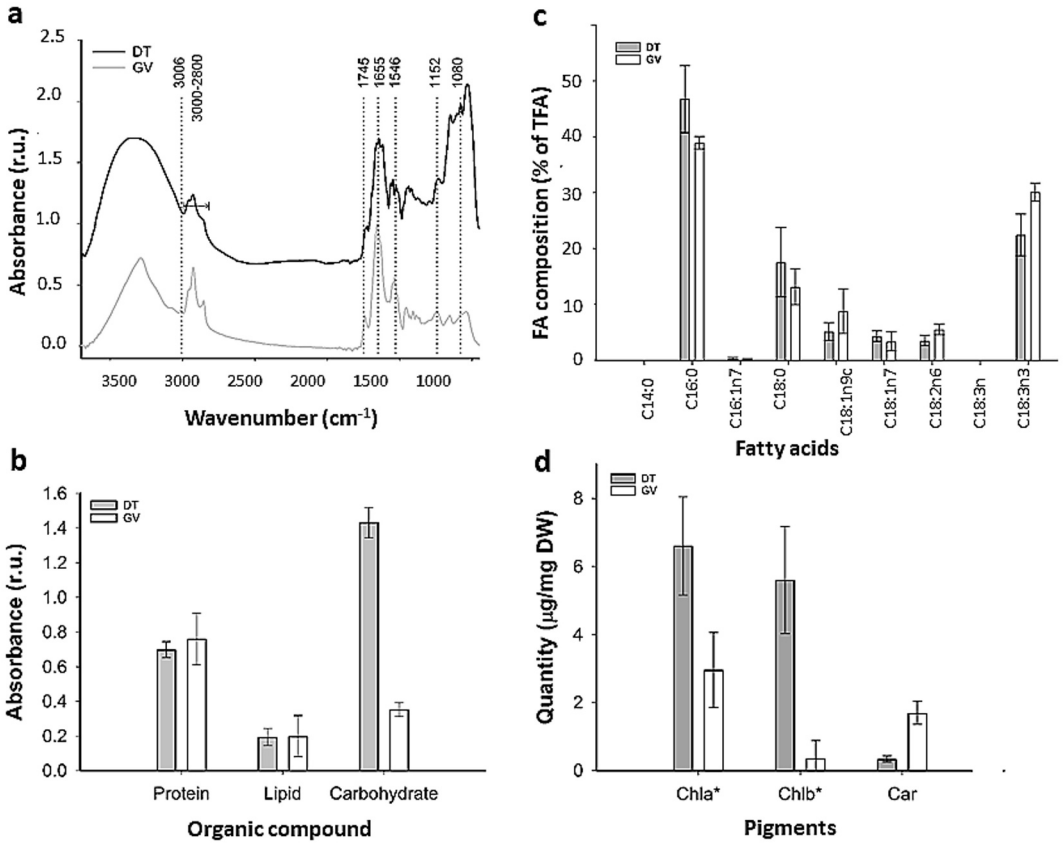

Fig. 1. Chemical characterization: FTIR spectra of DTs (gray line) and GVs (black line). The dotted vertical lines indicate the vibrational bands originating from the major macromolecules: cis double bond of fatty acids (~3006 cm^{-1}), asymmetric and symmetric vibrations of CH_3 and CH_2 of fatty acids (~3000–2800 cm^{-1}), lipids (1745 cm^{-1}), proteins (1655 cm^{-1}, 1546 cm^{-1}), nucleic acid/phosphate (1080 cm^{-1}), and carbohydrate (1152 cm^{-1}). Spectra have been shifted for better readability (a). Main organic compounds are expressed as ratios of macromolecules to Amide *I* for GVs and DTs (b), fatty acids for DTs and GVs (c), and chlorophyll and carotenoid content for DTs and GVs (d). Results are shown as the mean ± standard deviation (SD) of three independent isolations.

GVs showed that proteins were retained in the GVs, as indicated by the amide-II/amide-I ratio and a similar lipid/protein ratio. The vesicles contained significantly less carbohydrate compared to DT cells (Fig. 1b). The major fatty acid components in GVs were palmitic acid (C16:0) (38.9 ± 1.2)%, stearic acid (C18:0) (13.1 ± 3.2)%, and α-linolenic acid (C18:3n3) (30.1 ± 1.6)% of TFA. Other fatty acids, such as oleic acid (C18:1n9), cis-vaccenic acid (C18:1n7), and linoleic acid (C18:2n6), were maintained at or below 10% of TFA (Fig. 1c).

We detected four lipid classes of thylakoid origin - monogalactosyldiacylglycerol (MGDG), digalactosyldiacylglycerol (DGDG), sulfoquinovosyldiacylglycerol (SQDG), and phosphatidylglycerol (PG) - in the lipid extract of the isolated vesicles (Fig. S1). Polar lipids accounted for the majority of lipids in DTs and GVs, at (76.7 ± 0.5)% and (80.8 ± 0.7)% of total lipids, respectively. MGDG and PG were the major polar lipids in DTs and GVs, at (30.50 ± 0.06)% and (26.76 ± 0.85)%, respectively. PG contributed (16.8 ± 1.7)% and (21.46 ± 0.11)%, respectively. The ratios of lipid classes remained largely constant during membrane reconstruction, despite slight changes. Non-polar lipids were present but accounted for a lower percentage of the total lipid content, and lipid content differed between cellular and vesicular forms.

The pigment extracts of DTs and GVs differed both qualitatively and quantitatively. In GVs, the chlorophylls (Chl) were degraded to pheophorbides, as indicated by the absorption band at ~535 nm and the blue shift of the Soret band (350–425 nm) (Fig. S2a). Cells contained relatively high amounts of Chla and Chlb, (6.6 ± 1.5) and (5.6 ± 1.6) µg mg^{-1} DW, respectively (Fig. 1d). The GVs did not contain chlorophylls, but only their degradation products: pheophorbide a (Phea) (2.9 ± 1.1) µg mg^{-1} and even less pheophorbide b (Pheb) (0.36 ± 0.51) µg mg^{-1}. Carotenoids were present in higher amounts in the GVs fraction, reaching five times higher amounts of (1.70 ± 0.34) µg mg^{-1}, compared to DTs (0.34 ± 0.09) µg mg^{-1}. The total pigment content was about 2.5 times higher in DTs than in GVs, at (12.5 ± 3.0) and (5.0 ± 1.3) µg mg^{-1}, respectively. HPLC-DAD-FL analysis confirmed the presence of chlorophylls in DTs (vertical dotted lines 6 and 7, Fig. S2c) and the presence of chlorophyll degradation products in GVs (vertical dotted line 3, Fig. S2c). A total of five carotenoids were detected (Fig. S2b and S2c). HPLC confirmed the enrichment of GVs with carotenoids.

3.2. Morphological and optical features of microalgae-derived vesicles

Micrometer-sized GVs (prepared as described in Section 2.2) were sonicated to generate nanometer-sized vesicles. The morphology of the GVs was visualized using complementary imaging techniques: TEM, CLSM, and AFM. While AFM was used to characterize detailed morphological features, TEM was used as a high-throughput technique to rapidly assess the overall state of the vesicles after sonication. Fig. 2 presents representative high-contrast TEM images of a dense, heterogeneous population of reconstructed microalgae-derived vesicles, visually confirming successful size reduction and consistent sample quality before further experiments. Samples were negatively stained with UranyLess, which provides strong membrane contrast and supports the presence of closed vesicles rather than membrane debris.

This TEM image shows a field of spherical vesicles of varying sizes distributed throughout the grid. Analysis of 100 vesicles yielded an average diameter of (290 ± 19) nm. The left side exhibits the broadest area, with multiple vesicles of varying sizes. The central panel provides an enhanced perspective of bigger vesicles, and the right panel provides an enhanced view of tiny vesicles both showing the vesicles with clear

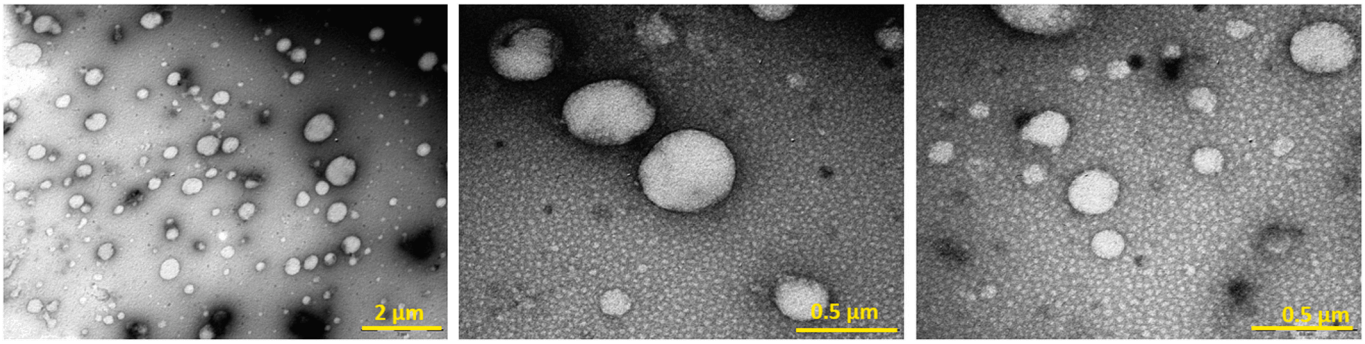

Fig. 2. TEM images of the GVs after sonication of the suspension. The vesicle suspension was contrasted with UranyLess™ contrast medium solution and washed in ultrapure water before visualization in TEM.

membrane boundaries regardless of the vesicle size.

To provide insight into micrometer-sized GVs and fluorophore distributions, confocal imaging was performed on nearly empty GVs of different sizes, revealing their natural autofluorescence (excitation: 450 nm, emission: 680 nm; Figs. S2, S3a). To understand the origin of this autofluorescence, we compared the fluorescence measurements of GVs and DTs. The results showed that the maximum fluorescence at both temperatures (77 K and room temperature) occurs at lower wavelengths, indicating that the pigments are free in GVs, in contrast to cells where the pigments are bound to the antenna complexes (Figs. S3b, S3c).

3.3. Mechanical and hydrophobic properties of microalgae-derived vesicles

To quantify the mechanical and hydrophobic properties of vesicles, AFM force spectroscopy was used. The elastic properties of the microalgae-derived vesicles were quantified using the apparent Young's modulus (E_{app}) at a 2 µm indentation depth. The apparent Young's modulus values likely indicate whether a micrometer-sized vesicle is empty or full: soft structures exhibited an elasticity modulus of (0.38 ± 0.18) kPa, while non-empty vesicles showed (1.51 ± 0.73) kPa. Such a low E_{app} value occurs because these vesicles are empty and large, so when a load is applied, the vesicle membrane is easily deformed. A similar trend in E_{app} for empty and loaded dipalmitoylphosphatidylcholine liposomes was observed [31]. Our data show no correlation between vesicle size and mechanical properties, which aligns with observations for extracellular vesicles from eukaryotic cells [32,33].

The hydrophobicity of GVs was previously determined using FluidFM with an air bubble, providing qualitative data [18,34]. Here, hydrophobicity measurements were conducted as previously reported for DT cells, using a chemically modified probe (Fig. S4) [35]. The maximum work of adhesion of vesicles on hydrophilic and hydrophobic probes is shown in Fig. 3.

The maximum work of adhesion measured in deionized water with a hydrophilic probe was (0.00357 ± 0.00051) fJ, compared to (0.000103 ± 0.000008) fJ for a hydrophobic probe (Fig. 3a). The adhesion probability between vesicles and the probe (the ratio of curves with adhesion events to the total number of curves) was 28% for hydrophilic probes and 22% for hydrophobic probes, consistent with a predominantly hydrophilic vesicle surface. The vesicles therefore showed a positive ΔW_{adh} of (0.00347 ± 0.00051) fJ, indicating hydrophilic nature (Fig. 3c).

In contrast to initial observations, independent hydrophobicity measurements in seawater revealed hydrophobic vesicle behaviour (Fig. 3b). The maximum work of adhesion with a hydrophilic probe was (0.110 ± 0.037) fJ, while with a hydrophobic probe it was (0.247 ± 0.040) fJ. The adhesion probability for vesicle binding to the hydrophilic probe was 46%. Adhesion to the hydrophobic surface occurred in 100% of curves. Along with the negative ΔW_{adh} value of (−0.133 ± 0.077) fJ, these results show that, under these conditions, the vesicles are hydrophobic (Fig. 3c). This highlights the role of cation-mediated charge modification.

3.4. Redox activity of microalgae-derived vesicles

In the initial spin labeling experiments, we observed a gradual loss of EPR signal intensity in both the DT samples and the GVs, regardless of the preparation method. However, signal decay was influenced by conditions such as isolation batch and storage time. The results of a systematic measurement of signal decay are shown in Fig. 4 for control samples, DT cells, and GVs, with the corresponding rate constants listed

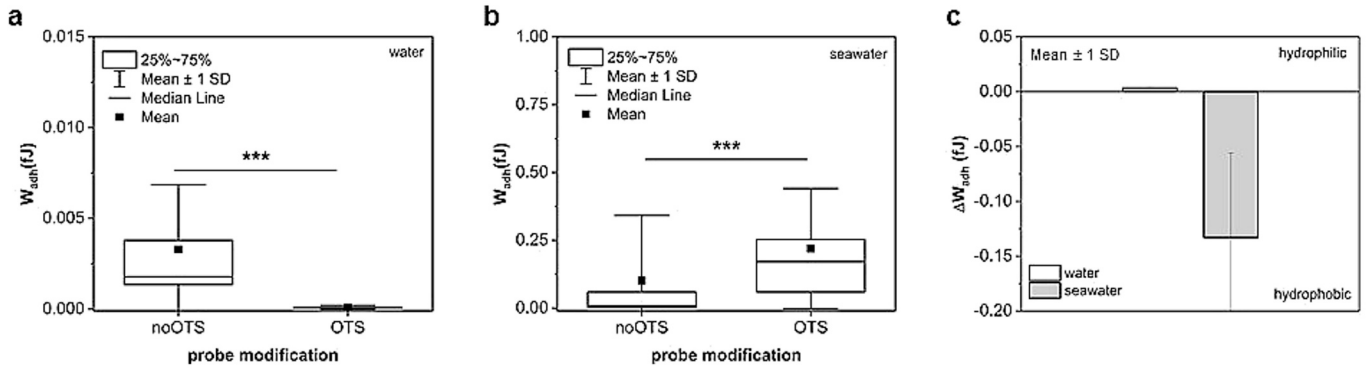

Fig. 3. AFM force spectroscopy: Maximum work of adhesion (W_{adh}) quantifying vesicle interaction with a hydrophilic (no OTS) and a hydrophobically functionalized (OTS) tip in deionized water (a) and seawater (b). Data are presented as box plots (25%–75%). Outliers standard deviations of the mean (black solid square), and the median is indicated by a horizontal line. Statistical difference was tested by Kruskal-Wallis ANOVA at the 0.05 level. Notation *** corresponds to $p < 0.001$. (c) The ratio of hydrophilic to hydrophobic properties of algae-derived vesicles in deionized water and seawater. Data are shown as maximum ΔW_{adh} ± maximum error.

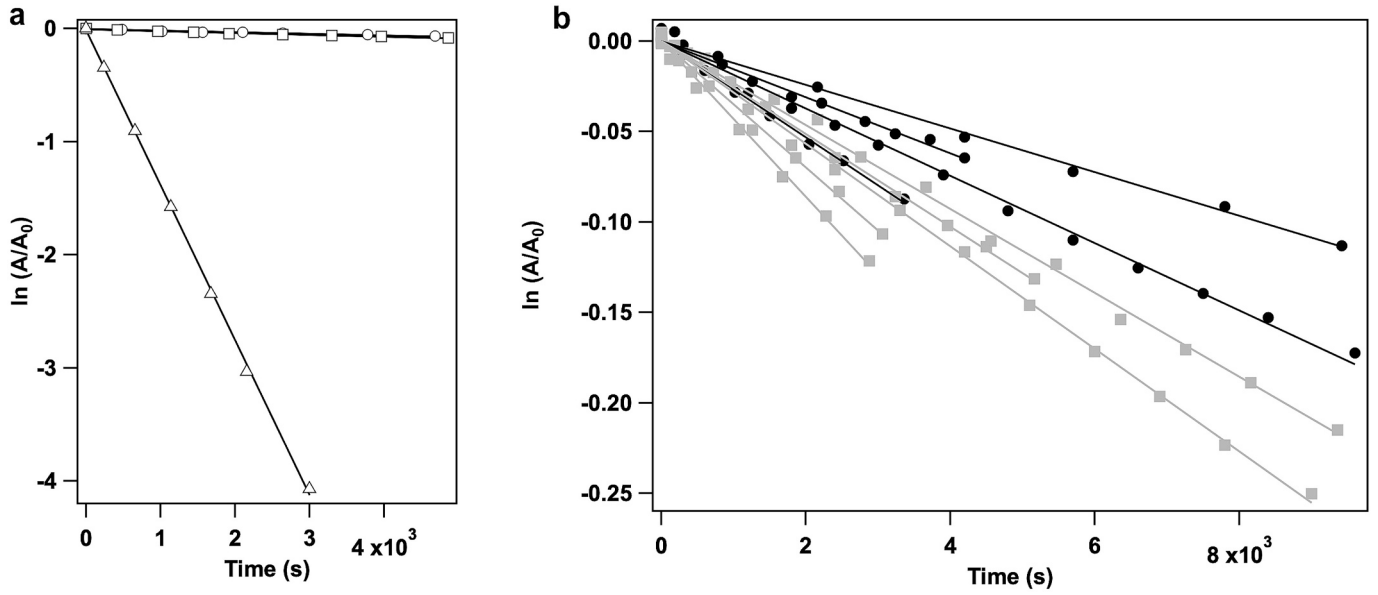

Fig. 4. Linearized EPR signal decays of TEMPO spin label in the presence of redox agents, DT cells, and GVs. (A) Control samples: 4×10^{-4} M TEMPO in ultrapure water (○), in 1×10^{-3} M H_2O_2 (□), and in 1×10^{-3} M ascorbic acid (△). (B) TEMPO in DT cell suspension (4×10^6 cells per sample) (●) and in GV suspension (10^{-6} GVs per sample, ■). Lines represent linear fits to the ln-linear data (the rate constants are presented in Table S1).

in Table S1.

In principle, the loss of EPR signal from the spin label could result from either reduction or oxidation of its doxyl group. To determine whether the signal decay was caused by reduction or oxidation of the spin labels, we treated the samples with H_2O_2 (an oxidizing agent) and ascorbic acid (a reducing agent). A marginal decay of TEMPO in water was observed both in the absence and presence of H_2O_2, indicating that the oxidizing agent cannot effectively oxidize TEMPO. In contrast, ascorbic acid rapidly reduced the spin label, resulting in a much faster decay of the TEMPO signal in water, with a rate constant approximately two orders of magnitude higher. TEMPO in the suspension of DT cells (4×10^6 cells per sample) showed somewhat faster decay than the corresponding control samples. Most interestingly, TEMPO in the GVs suspension (1×10^6 GVs per sample) showed a faster decay than the DT cells. Considering that we had four times fewer GVs per sample than DT cells the data in Table S1 show that the GVs have significantly ($p < 0.05$) higher antioxidant capacity than the isolated and purified DT cells ($SE_{diff} = 8.16 \times 10^{-6}$, $t = 3.25$).

3.5. Cytotoxicity and immunogenicity assessment

The GVs did not cause substantial cytotoxicity in the selected cell lines and at the concentrations tested (Fig. 5a).

Detroit 562 cells were the most sensitive, as even the lowest

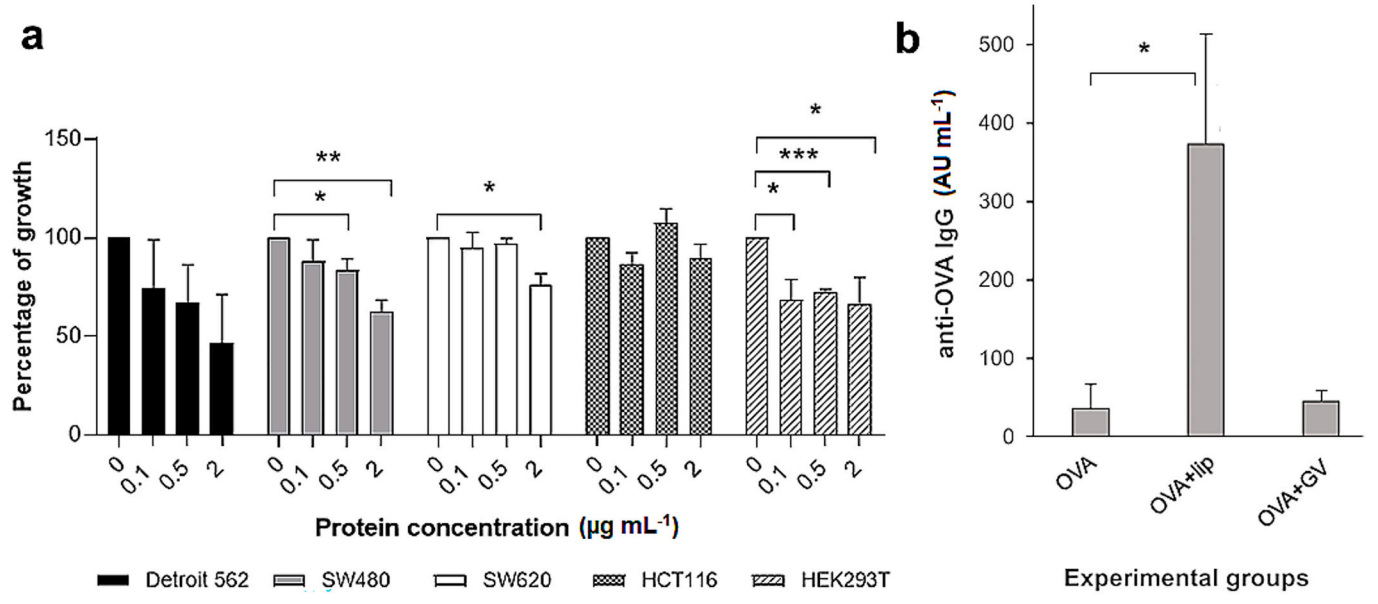

Fig. 5. Cytotoxicity assay on selected cell lines (a): pharynx carcinoma (Detroit 562), colon carcinoma (SW480, SW620, HCT116), and human embryonal kidney carcinoma (HEK293T) (Student's *t*-test, * $p < 0.05$, ** $p < 0.01$, *** $p < 0.005$). Immunogenicity (b): The amount of total anti-OVA IgGs in the sera of NIH/OlaHsd female mice ($n = 5$). The experimental groups were: OVA in saline, OVA in liposomes, and OVA in GVs. Anti-OVA antibodies were determined using ELISA. The one-way ANOVA test revealed a statistical significance of the mean values between OVA+lip and OVA (control) at the 0.05 level (* $p < 0.05$).

concentration used caused a 30% reduction in proliferation, although this was not statistically significant. For SW480 and SW620, only the highest concentration (2 μg mL^{-1}) caused cytotoxicity, but even at this concentration, 60% of cells survived. HCT116 was the most resistant cell line, with no concentration causing a statistically significant decrease in cell numbers. The decrease in HEK293T cell numbers reached statistical significance, but the small magnitude of change indicates no substantial cytotoxic effect, especially as it was not concentration-dependent. The percentage of surviving cells was (68 ± 10.4) %, (72 ± 1.94) %, and (67 ± 13.27) % when treated with 0.1, 0.5, and 2.0 μg mL^{-1} vesicles, respectively. These results suggest that factors other than GVs exerted a primary influence on cell survival, possibly residual bioactive remnants.

An immunogenicity study was performed in a mouse model to determine whether the GVs affect the immune system (Fig. 5b). In particular, the GVs were examined for the induction of systematic immune responses against the model antigen ovalbumin. NIH/OlaHsd mice were immunized with ovalbumin-containing GVs.

To understand the nature of these induced immune responses with respect to Th1/Th2 polarization, the levels of Th1-associated IgG2a and Th2-associated IgG1 antibody isotypes were also measured as shown in Fig. S5, [36]. However, there were no significant differences in the increase in IgG production. Liposomes trigger a predominantly Th2-oriented reaction with a significant increase in IgG1 production and only a marginal increase in IgG2a compared to the control antigen in saline solution. The formulation of the antigen in GVs slightly increased the humoral immune response and the production of anti-OVA antibodies (Fig. 5b).

3.6. Cargo–membrane association of reconstructed microalgae-derived vesicles

For better visualization and possible colocalization, the GVs were stained with the lipophilic dye DiI, which selectively stains lipid moieties and emits a strong red fluorescence (with maximum absorption at 549 nm and emission at 565 nm). Fig. 6 shows representative reconstructed microalgae-derived vesicles stained with DiI before and after the addition of model drugs.

Before the drug addition, the DiI-stained GVs showed a uniform lipid arrangement within the reconstructed membrane. Two drugs, vancomycin-FITC and oligo-DNA-FAM (which mimics DNA-based aptamers), labeled with green fluorescein dyes, have different physicochemical properties and versatile applications (Table 1).

Accumulation of the drug within the membrane rim was visualized by green fluorescence, which effectively colocalized with the red fluorescence of DiI, while the vesicle interior and background did not fluoresce. Vancomycin-FITC rapidly accumulates on the membranes of the GVs, and retains a high and persistent fluorescence intensity even after 2 h and subsequent rinsing of the samples. In contrast, although oligo-

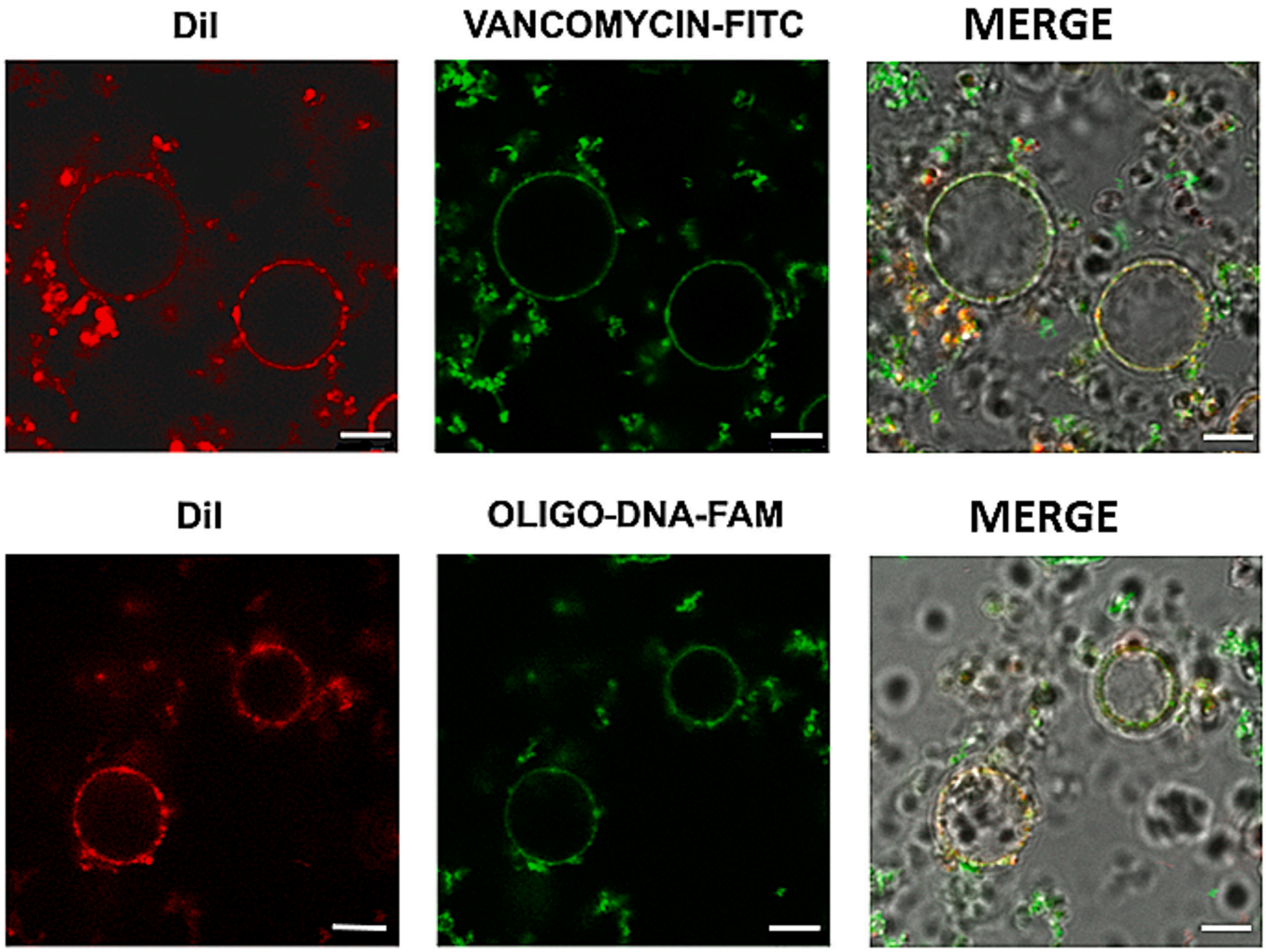

Fig. 6. Cargo-membrane association: GVs stained with DiI (red) after the addition of vancomycin-FITC and oligo-DNA-FAM (green). The merged images show the colocalization of the fluorescently labeled drugs with the vesicle membrane. The scale bar represents 5 μm. (For interpretation of the references to colour in this figure legend, the reader is referred to the web version of this article.)

DNA-FAM accumulates similarly on the membrane, a significant increase in fluorescence was observed after sample rinsing alone. We also observed that debris surrounding the GVs showed fluorescence, although its intensity varied with both drugs.

3.7. Additional evaluation of structural recovery and stability

To assess the material's long-term storage viability, an additional characterization was performed on the post-processed vesicle sample (protocol described in Section 2.3). AFM imaging was used to determine whether the dried membrane fragments retain their ability to successfully and reversibly self-assemble into well-defined vesicular structures. Representative AFM topography images of this formulation, recorded in both air and liquid environments, are shown in Fig. S6, highlighting the recovered spherical morphology. Quantitative analysis showed that the average diameter and height of the vesicles imaged in air were (160 ± 22) nm and (30 ± 7) nm, respectively. In a liquid medium, their average diameter and height were measured at (172 ± 26) nm and (33 ± 7) nm, respectively. Although characterized in detail elsewhere [40], current results indicate the structural recovery and shelf-life potential of this matrix.

4. Discussion

4.1. Self-assembly of reconstructed microalgae-derived vesicles

To create a model membrane system that closely mimics natural biological membranes, a promising approach involves emptying the cell interior [37]. This principle, originally utilized to produce ghost vesicles (GVs) from osmotically unstable erythrocytes, is highly applicable to specific microalgal species due to their similarly low cellular stiffness, which is a prerequisite for effective vesicle formation [38,39]. When these highly deformable cells are exposed to hypoosmotic stress, rapid swelling and increased membrane tension lead to pore formation and subsequent cell rupture. Upon the release of intracellular contents, the remaining membrane fragments spontaneously fuse through non-covalent interactions to form multicomponent GVs, a self-assembly process that remains poorly understood due to the scarcity of literature on microalgae-derived systems.

In our previous work, we successfully established an osmotic-shock protocol to isolate these algal plasma membrane vesicles, validating their inherent autofluorescence and providing initial structural and permeability insights via atomic force microscopy (AFM) and confocal laser scanning microscopy (CLSM) in comparison to model DOPC giant unilamellar vesicles (GUVs) [17]. We subsequently extended this concept through a detailed biophysical characterization of their morphology, lipid and protein composition, nanomechanics, and permeability to fluorescent probes, demonstrating that these reconstructed vesicles are soft, hydrophilic, and capable of size-selective cargo transport [18].

The present study significantly advances these earlier reports by employing an integrated framework that combines biological bottom-up ("bio-manufacturing") and biophysical top-down (hypoosmotic cell disruption) strategies. Given the complexity of this lipid-protein matrix, we use a comprehensive set of techniques (TEM, AFM in air and liquid, CLSM, FTIR, GC-FID, and HPLC) to simultaneously resolve vesicle morphology, biochemical composition, and nanomechanical properties. Utilizing AFM-based force spectroscopy with modified and unmodified probes [35], the surface hydrophilicity of the GVs was directly correlated with their parental cells, while also revealing a distinct stiffness differentiation between nearly empty and nonempty vesicles for the first time. Furthermore, this work provides the first preliminary evaluation of the *in vitro* cytotoxicity, *in vivo* immunogenic profile, and surface-mediated noncovalent cargo-loading capacity for a glycopeptide antibiotic and an oligonucleotide. Enhanced antioxidant activity was likewise observed in GVs compared to parental cells, correlating with a distinct carotenoid enrichment. Finally, to achieve a stable and practically applicable format, the role of lyophilization was evaluated as a crucial stability test. Although dry storage may limit the detection of unstable RNA and slightly decrease antioxidant activity [40], it demonstrates that the complex matrix can successfully reassemble upon reconstitution. The following section explores how these vesicles remodel and mimic parental cell properties.

4.2. Reconstructed microalgae-derived vesicles mimic microalgae properties

Reconstructed microalgae-derived vesicles constitute a diverse population characterized by morphological and stiffness variations ranging from nearly empty to non-empty vesicles, a feature intrinsic to spontaneous membrane self-assembly from complex marine biomass. This structural heterogeneity may be attributed to suboptimal synchronization of cell age within the population, protein fluctuations in different cell regions (apical versus basal body [7]), and an uneven salinity gradient. Vesicles that are mostly empty exhibit significant softness and have membrane heights of (15–20) nm, which could correspond to a surface globular structure, mainly membrane-associated proteins with diverse functions. Previously identified proteins in GVs originate mainly from the cytoplasm and chloroplasts and are involved in carbohydrate metabolism, amino acid biosynthesis, photosynthesis, oxidoreductase activity, and microtubule-based processes, which may contribute to vesicle stability [18,41]. In contrast, non-empty vesicles can reach heights of up to 60 nm due to residual intracellular material. Beside intact vesicles, a fraction of cellular debris is inherently present in the sample. In this study, our separation protocol was specifically optimized to remove the majority of heavy cellular fragments and dense debris without compromising the fragile vesicle structure. Further isolation by density-gradient centrifugation (e.g., sucrose gradients) was intentionally avoided in this workflow to prevent unwanted membrane modifications. Because these multi-component, reconstructed vesicles are highly osmotically sensitive and structurally fragile, exposing them to hyperosmotic sugar matrices or excessive high-speed shear stress would induce structural deformation and drastically reduce vesicle yield, altering the very membrane properties we aim to study. Crucially, the successful evacuation of internal cellular content during this workflow is verified by the drastic depletion of soluble carbohydrates (glucose, galactose, and rhamnose) and intracellular starch in the GV samples [42]. This biochemical change confirms the reduction of parental cytosol. This ensures that downstream functional traits such as cytotoxicity, redox and cargo-membrane association assays mainly reflect the intrinsic properties of the reconstructed vesicle matrix, rather than the effect of minor cytosolic remnants.

This structural remodeling is further evidenced by the fate of intracellular pigments during the workflow. In intact cells, chlorophyll molecules are stabilized within the large photosynthetic light-harvesting complexes (i.e. PSI and PSII antennae), but upon cellular disruption these macromolecular assemblies dissociate, and the unprotected chlorophyll rapidly degrades as indicated by the detection of its degradation products. Rather than a failure of assembly, this transition signifies the definitive disassembly of the native photosynthetic machinery, and the subsequent bottom-up reorganization into a biomimetic membrane matrix. Simultaneously, the strong retention of hydrophobic carotenoids within the GVs indicates their selective stabilization and integration within the newly formed lipid bilayer architecture.

The vesicle size measured by AFM in liquid was (172 ± 26) nm. In contrast, DLS experiments of the identical system yielded a hydrodynamic diameter of (215 ± 6) nm [40]. The reduced AFM values indicate partial deformation of soft vesicles on the substrate, whereas DLS also accounts for the surrounding hydration and ionic layer. In the non-optical AFM surface approach, vesicle size is obtained from cross-sectional analysis of the topographic image of individual vesicles (Fig. S6). Conversely, the optical bulk DLS technique measures the

autocorrelation function of laser light scattered at a fixed angle to determine the diffusion coefficient, which is then used to calculate the hydrodynamic diameter. The vesicle size determined by DLS may be greater as diffusion depends on interfacial characteristics [43]. The dimensions and interfacial characteristics are critically important for drug administration, since vesicles measuring 50–200 nm exhibit advantageous barrier penetration, cellular uptake, and circulation times.

Besides structural features and dimensions, the functional activity of the reconstructed vesicles was also evaluated through their interaction with radical probes. The observed decrease in EPR signal intensity of the spin label is in agreement with data previously reported for *Dunaliella primolecta* [44] and shows that both DT cells and GVs are able to reduce spin labels through membrane components. EPR measurements in this study showed significantly faster reduction kinetics of spin labels in the presence of GVs than in the presence of DT cells (Fig. 4, Table S1). To interpret this trend accurately, a key methodological aspect must be considered. As shown by the chemical characterization (Section 3.1), the antioxidant capacity of both DT cells and GVs arises from a complex matrix of bioactive compounds, including enriched carotenoids, specific polyunsaturated fatty acids (such linolenic acid), and thylakoid-derived polar lipids (MGDG, DGDG, PG; Figs. 1, S1, S2), along with membrane-associated proteins and other antioxidant constituents. Because these diverse components contribute collectively and synergistically to the overall redox activity, absolute quantification calibrated against a single compound for normalization would be arbitrary and would not capture the holistic contribution of the reorganized matrix. Therefore, a robust semi-quantitative approach comparing the EPR signal reduction rates on a per-particle basis (DT cells vs. GVs) was adopted. We hypothesize that this increased reduction rate per particle for GVs is directly driven by macromolecular reorganization during vesicle reconstruction. In intact DT cells, many antioxidant and redox-active components are buried within complex intracellular structures (such as thylakoid membranes and chloroplasts), which partially shield them from external molecules. Upon cellular disruption and subsequent self-assembly into GVs, these components become inverted or directly oriented on the highly curved, high-surface-area vesicle membrane, greatly increasing the physical accessibility of the active moieties to external radical probes like TEMPO. Although EPR is a bulk technique capturing the cumulative response of the entire sample, this observed doubling of the reduction rate cannot be explained by the mere presence of passive, amorphous cellular remnants. Indeed, if the sample consisted solely of non-reconstructed debris, random aggregation would limit the active surface area, making the reduction kinetics significantly slower. This kinetic acceleration, therefore, serves as a direct biophysical indicator of efficient, membrane self-assembly.

To ensure that downstream biological and functional claims are confidently linked to structurally intact systems rather than contaminating remnants, a multi-scale characterization approach was employed. At the single-vesicle level, CLSM, negative staining TEM (with UranyLess), and AFM allowed us to explicitly distinguish intact, closed vesicular boundaries from amorphous debris, confirming that the analyzed populations consist predominantly of well-defined vesicles. This microscopic imaging evidence was independently validated by small-angle neutron scattering analyses on the identical system, providing unambiguous physical proof of intact, closed lamellar structures as a bulk property in the native fluid state [40].

The structural integrity of this closed bilayer barrier is independently supported by permeability assays, which demonstrate clear size-selective permeability to dextrans [18]. Crucially, because the loading of therapeutic cargo or macromolecules is achieved via passive incubation, these molecules undergo non-covalent adsorption and specific surface binding to the highly organized vesicle interface, rather than internal encapsulation within the aqueous core. This capacity for stable surface binding and interfacial retention has been explicitly confirmed for macrocyclic peptides and oligonucleotides strictly at the vesicle boundary, proving that the reconstructed membrane architecture offers a functional and predictable platform for surface-associated cargo delivery. This preserved and fluid membrane organization is further supported by findings [40] that GVs successfully retain the original membrane dynamics of DT cells, likely determined by the specific degree of lipid chain saturation (Fig. 1). Here, polar lipids dominate the total lipid pool, supporting membrane integrity, fusion, fluidity, and overall hydrophilicity, which aligns with previous lipid-class investigations indicating that the relative distribution of lipid classes is mostly preserved between parental cells and GVs [18].

Fine tuning of GV properties can further be achieved by changing the growth conditions of the parent cells. Cells of DT were reported to alter its lipid composition with respect to temperature and salinity changes, resulting in a change of its stiffness and surface hydrophobicity [26,35,45]. Furthermore, cell stiffness and hydrophobicity are highly variable between growth phases [46]. The timing of cell harvest is critical to minimize batch-to-batch variability and to maintain membrane reconstruction efficiency. For example, DT cells collected in the stationary phase are softer and more hydrophilic than DT cells collected in the exponential growth phase, resulting in increased sensitivity of cells to osmotic shock and bottom-up membrane self-assembly.

Besides intrinsic cell properties, the external medium determine the vesicle features. GVs are hydrophilic in water and phosphate-buffered saline, but exposure to seawater, which has higher ionic strength and concentrations of divalent cations, significantly reduces the overall surface charge and drives the vesicles toward a more hydrophobic state.

This research presents a laboratory-scale proof of concept that provides a strong foundation for addressing intrinsic system limitations. We have confirmed the structural and functional integrity of the vesicles; however, a natural degree of heterogeneity remains an expected and inherent feature of spontaneous self-assembly from complex natural sources. This variation arises not only from biological differences in the starting cell culture but also because the vesicles originate from different cellular membrane compartments with distinct compositions. Consequently, comprehensive quantification of batch purity, along with the development of alternative non-destructive purification and encapsulation strategies, represents the next step in our research to advance this platform toward validated delivery applications.

4.3. Biocompatibility and cargo binding of microalgae-derived vesicles

A comprehensive preliminary assessment of the *in vitro* cytotoxicity and *in vivo* immunogenicity was carried out to evaluate the potential of these reconstructed vesicles as drug delivery platforms. Our *in vitro* screening revealed a very promising safety profile in different human cell lines (Fig. 5a), with overall reductions in cell proliferation well within the limits accepted for acute cytotoxicity. However, some line-specific sensitivities were observed. For example, Detroit 562 pharyngeal carcinoma cells were the most sensitive, whereas the colorectal lines SW480 and SW620 only dropped to about 60% survival at the highest concentration (2 μg mL^{-1}). In contrast, HCT116 cells remained highly resistant across all tested doses. Interestingly, while the immortalized embryonic kidney line HEK293T commonly employed in the literature as a standard non-tumor comparator [47–49], showed a statistically significant decrease in cell numbers, the effect size was modest (~67–72% viability) and notably independent of vesicle concentration.

These findings are broadly in line with previous reports on algae-based systems, such as nanoalgosomes [14], in specific effects of *Spirulina platensis* on epithelial and colorectal carcinoma cell lines [45,46]. Importantly, the minor and often non-concentration-dependent effects on cell viability indicate that factors other than the vesicle platforms per se exerted a primary impact. This is likely due to minor, residual bioactive remnants from the *D. tertiolecta* cell culture (such as pigments or fatty acids) that possess intrinsic biological activity [50].

Immunogenicity is a major concern in biotherapeutics and will also be critical for drug delivery systems based on natural materials [51]. Clinical data on the immunogenicity of carriers remain limited and

primarily focus on liposomes, where immune responses are complex and multifactorial [52]. Encapsulation of OVA in GVs produced only a modest increase in the humoral immune response and anti-OVA antibody levels, indicating that GVs act as a mild adjuvant rather than a strong immunostimulant. These preliminary findings establish a baseline for more comprehensive, long-term immunogenicity evaluations.

Vesicle morphology and interfacial characteristics [53] determine drug release kinetics, therapeutic effectiveness, and ability to overcome biological barriers to provide effective, safe, and regulated drug delivery [54,55]. Extensive studies on various cell-based materials demonstrate their significant potential for drug delivery due to their ability to mimic natural biological membranes [56–61]. In this laboratory study, we used microalgae derived vesicles to test the binding of two distinct model drugs: a large, flexible macrocyclic peptide (vancomycin FITC) and a short exogenous DNA (oligo DNA FAM), Fig. 6. Because macromolecular loading was performed via passive incubation, the cargo specifically adsorbs and binds non-covalently to the organized vesicle interface rather than being enclosed within the aqueous core, an observation consistent with independent studies [18,40]. The first model drug, vancomycin, is a clinically important glycopeptide antibiotic used against methicillin-resistant *Staphylococcus aureus*. It binds to the D-Ala-D-Ala terminus of the bacterial peptidoglycan precursor, thereby hindering cell wall synthesis and causing cell lysis [62]. Under our experimental conditions, the labeled vancomycin behaves as a hydrophilic molecule (Table 1). Given the measured suspension pH of 6.68, vancomycin carries a partial positive charge, suggesting that electrostatic attraction, potentially modulated by residual cations from disrupted cells, drives its association with the negatively charged vesicle membrane. Notably, while previous strategies covalently attached vancomycin to whole algal cells via click chemistry and cleavable linkers for UVA1-irradiated controlled release [63], our system uniquely relies on purely non-covalent membrane binding. The second model drug, oligo-DNA-FAM, was selected to mimic therapeutic DNA-based aptamers. Although both DNA and the vesicle membrane are negatively charged, cytoplasm-derived cations partially screen these surface charges. This screening allows electrostatic interactions between the DNA and the positively charged choline headgroups, further stabilized by hydrogen bonding and hydrophobic interactions. An increase in the external calcium concentration did not enhance binding, showing that endogenous cation levels were already enough for charge compensation. Despite its short length (12 bp), oligo-DNA-FAM mostly bound to the surface of the permeable membrane, emphasizing the large potential of these GVs to act as nucleic acid carriers.

5. Conclusions

The marine microalga *Dunaliella tertiolecta* serves as a sustainable, environmentally friendly cell template for the spontaneous reconstruction of cell-sized vesicles from native lipid, protein, and pigment matrices. Biophysical screening of this complex, multicomponent system reveal structural features of vesicles that govern their potential function. Vesicles can be readily resized due to their low mechanical stiffness. The presence of polar lipids and a balanced ratio of saturated and unsaturated fatty acids allows the maintenance of membrane integrity and fluidity. The ratio of protein to lipid is essentially preserved in DT cells and GVs, indicating an efficient reconstruction process. The interfacial properties of vesicles are also strongly influenced by their environment, being hydrophilic in water and hydrophobic in seawater. The structural integration of chlorophyll breakdown products and carotenoids within the membrane dramatically increases the antioxidant potential of the vesicle, resulting in efficient radical scavenging action at the membrane interface.

The reconstructed vesicles proved to be biocompatible, exhibiting no acute cytotoxicity *in vitro* and only mild adjuvant activity *in vivo*. Functionality assays confirm that both a macrocyclic glycopeptide antibiotic and an oligonucleotide can successfully bind to the vesicle membrane via non-covalent interactions. To advance the practical handling and shelf-life of this system a robust lyophilization and rehydration strategy was established, proving that the material preserves its morphology and capacity for membrane self-assembly upon reconstruction.

The results support the use of reconstructed microalgae-derived vesicles as a versatile platform for the development of next-generation sustainable and safe delivery systems for human health, food technology and environmental remediation. Although population heterogeneity and polydispersity remain intrinsic limitations of spontaneous bottom-up self-assembly from complex marine biomass at this laboratory proof-of-concept stage, they provide a basis for further optimization. Therefore, the next steps to advance this platform toward validated delivery applications include thorough quantification of batch quality and the development of alternative, non-destructive purification and cargo-loading strategies.

CRediT authorship contribution statement

Nadica Ivošević DeNardis: Writing – review & editing, Writing – original draft, Visualization, Validation, Supervision, Resources, Project administration, Methodology, Investigation, Funding acquisition, Conceptualization. **Tea Mišić Radić:** Writing – review & editing, Writing – original draft, Visualization, Validation, Methodology, Investigation. **Mária Klacsová:** Writing – review & editing, Writing – original draft, Visualization, Validation, Methodology, Investigation, Formal analysis, Data curation, Conceptualization. **Daniela Uhríková:** Writing – review & editing, Writing – original draft, Visualization, Validation, Methodology, Investigation, Formal analysis, Data curation, Conceptualization. **Ruža Frkanec:** Writing – review & editing, Writing – original draft, Visualization, Validation, Methodology, Investigation, Formal analysis, Data curation, Conceptualization. **Joanna Zemła:** Writing – review & editing, Writing – original draft, Visualization, Validation, Methodology, Investigation, Formal analysis, Data curation, Conceptualization. **Malgorzata Lekka:** Writing – review & editing, Writing – original draft, Visualization, Validation, Methodology, Investigation. **Martin Lukeš:** Writing – review & editing, Writing – original draft, Visualization, Validation, Methodology, Investigation, Formal analysis, Data curation, Conceptualization. **Ondrej Prášil:** Writing – review & editing, Writing – original draft, Visualization, Validation, Methodology, Investigation. **Krisztina Sebők-Nagy:** Writing – review & editing, Writing – original draft, Visualization, Validation, Methodology, Formal analysis, Data curation. **Tibor Páli:** Writing – review & editing, Writing – original draft, Visualization, Validation, Methodology, Investigation, Formal analysis, Data curation, Conceptualization. **Katarina Lisac:** Writing – review & editing, Writing – original draft, Visualization, Validation, Methodology, Formal analysis, Data curation. **Marcela Chovancová:** Writing – review & editing, Visualization, Formal analysis. **Karlo Ojdanić:** Writing – review & editing, Writing – original draft, Visualization, Validation, Methodology, Formal analysis, Data curation. **Lucija Horvat:** Writing – review & editing, Visualization, Formal analysis. **Petra Peharec Štefanić:** Writing – review & editing, Writing – original draft, Visualization, Validation, Methodology, Formal analysis, Data curation. **Kristina Smokrović:** Writing – review & editing, Visualization, Formal analysis. **Nadica Maltar-Strmečki:** Writing – review & editing, Writing – original draft, Visualization, Validation, Methodology, Investigation, Formal analysis, Data curation, Conceptualization. **Dijana Pavlović Saftić:** Writing – review & editing, Writing – original draft, Visualization, Validation, Methodology, Formal analysis, Data curation. **Ivo Piantanida:** Writing – review & editing, Writing – original draft, Visualization, Validation, Methodology, Investigation. **Tanja Matijević Glavan:** Writing – review & editing, Writing – original draft, Visualization, Validation, Methodology, Investigation, Formal analysis, Data curation, Conceptualization.

Ethical approval

Ethical approval was obtained from the Ethics Committee of the Institute of Immunology and the Directorate of Veterinary and Food Safety of the Ministry of Agriculture of the Republic of Croatia (protocol title: "Razvoj adjuvanata nove generacije temeljenih na derivatima glikopeptida i nanosustavima za dostavu cjepiva", approval number: HR-POK-009).

Funding

We thank the International Visegrad Fund for financially supporting the project "Research network V4-Croatia for the development of novel drug carriers from algae" (ID 22220115).

Declaration of competing interest

The authors declare no competing interests.

Acknowledgments

We thank Nives Novosel Vlašić for sample preparation in the initial phase and Tanja Jurkin for preliminary DLS measurements. N.I.D. thanks P. Thomas Vernier for insightful discussions during the initial stage of this work. We also thank the anonymous reviewers for their valuable comments and constructive suggestions, which improved the quality and clarity of this manuscript.

Appendix A. Supplementary data

Supplementary data to this article can be found online at https://doi.org/10.1016/j.algal.2026.104852.

Data availability

Data will be made available on request.

References

[1] M. Silva, D. Avni, J. Varela, L. Barreira, The ocean's pharmacy: health discoveries in marine algae, Molecules 29 (2024) 1900, https://doi.org/10.3390/molecules29081900.
[2] S. Rosales-Mendoza, Algae-based Biopharmaceuticals, first ed., Springer International Publishing, Cham, 2016.
[3] A. Rotter, M. Barbier, F. Bertoni, A.M. Bones, M.L. Cancela, J. Carlsson, M. F. Carvalho, M. Cegłowska, J. Chirivella-Martorell, M. Conk Dalay, M. Cueto, T. Dailianis, I. Deniz, A.R. Díaz-Marrero, D. Drakulović, A. Dubnika, C. Edwards, H. Einarsson, A. Erdoğan, O.T. Eroldoğan, D. Ezra, S. Fazi, R.J. Fitzgerald, L. M. Gargan, S.P. Gaudêncio, M. Gligora Udovič, N. Ivošević DeNardis, R. Jónsdóttir, M. Kataržytė, K. Klun, J. Kotta, L. Ktari, Z. Ljubešić, L. Lukić Bilela, M. Mandalakis, A. Massa-Gallucci, I. Matijošytė, H. Mazur-Marzec, M. Mehiri, S.L. Nielsen, L. Novoveská, D. Overlingė, G. Perale, P. Ramasamy, C. Rebours, T. Reinsch, F. Reyes, B. Rinkevich, J. Robbens, E. Röttinger, V. Rudovica, J. Sabotič, I. Safarik, S. Talve, D. Tasdemir, X. Theodotou Schneider, O.P. Thomas, A. Toruńska-Sitarz, G.C. Varese, M.I. Vasquez, The essentials of marine biotechnology, Front. Mar. Sci. 8 (2021) 629629, https://doi.org/10.3389/fmars.2021.629629.
[4] S.N. Hazwani Oslan, N.J. Xuan, F.A. Khodzori, B.N. Abdul Hakim, N. Huda, N. Julmohamad, N. Barzkar, Comprehensive review of bioactive compounds from microalgae as promising source for industrial applications, Algal Res. 92 (2025) 104420, https://doi.org/10.1016/j.algal.2025.104420.
[5] G. Dolci, S. Puricelli, I. Crippa, L. Rigamonti, M. Grosso, Microalgae valorisation in different production sectors: a systematic review of life cycle assessment studies, Algal Res. 92 (2025) 104377, https://doi.org/10.1016/j.algal.2025.104377.
[6] A. Ahmad, S.S. Ashraf, Sustainable food and feed sources from microalgae: food security and the circular bioeconomy, Algal Res. 74 (2023) 103185, https://doi.org/10.1016/j.algal.2023.103185.
[7] A. Ben-Amotz, J.E.W. Polle, D.V. Subba Rao, The alga *Dunaliella*, first ed., Science Publishers, Enfield, New Hampshire, USA, 2009.
[8] I.S. Shchelik, S. Sieber, K. Gademann, Green algae as a drug delivery system for the controlled release of antibiotics, Chemistry (Weinheim an der Bergstrasse, Germany) 26 (2020) 16644–16648, https://doi.org/10.1002/chem.202003821.
[9] N.S. Sambudi, S. Cho, K. Cho, Porous hollow hydroxyapatite microspheres synthesized by spray pyrolysis using a microalga template: preparation, drug delivery, and bioactivity, RSC Adv. 6 (2016) 43041–43048, https://doi.org/10.1039/C6RA03147A.
[10] J. Delasoie, P. Schiel, S. Vojnovic, J. Nikodinovic-Runic, F. Zobi, Photoactivatable surface-functionalized diatom microalgae for colorectal cancer targeted delivery and enhanced cytotoxicity of anticancer complexes, Pharmaceutics 12 (2020) 480, https://doi.org/10.3390/pharmaceutics12050480.
[11] C. Tramontano, G. Chianese, M. Terracciano, L. de Stefano, I. Rea, Nanostructured biosilica of diatoms: from water world to biomedical applications, Appl. Sci. 10 (2020) 6811, https://doi.org/10.3390/app10196811.
[12] H. Huang, Y. Lang, S. Wang, M. Zhou, Microalgae-based drug delivery systems in biomedical applications, Eng. Regen. 5 (2024) 261–374, https://doi.org/10.1016/j.engreg.2024.01.002.
[13] I. García-Silva, M. Olvera-Sosa, B. Ortega-Berlanga, V. Ruíz-Rodríguez, G. Palestino, S. Rosales-Mendoza, Synthesis and characterization of innovative microgels based on polyacrylic acid and microalgae cell wall and their potential as antigen delivery vehicles, Pharmaceutics 15 (2022) 133, https://doi.org/10.3390/pharmaceutics15010133.
[14] G. Adamo, D. Fierli, D.P. Romancino, S. Picciotto, M.E. Barone, A. Aranyos, D. Božič, S. Morsbach, S. Raccosta, C. Stanly, C. Paganini, M. Gai, A. Cusimano, V. Martorana, R. Noto, R. Carrotta, F. Librizzi, L. Randazzo, R. Parkes, U. Capasso Palmiero, E. Rao, A. Paterna, P. Santonicola, A. Iglič, L. Corcuera, A. Kisslinger, E. Di Schiavi, G.L. Liguori, K. Landfester, V. Kralj-Iglič, P. Arosio, G. Pocsfalvi, N. Touzet, M. Manno, A. Bongiovanni, Nanoalgosomes: introducing extracellular vesicles produced by microalgae, J. Extracell. Vesicles 10 (2021) e12081, https://doi.org/10.1002/jev2.12081.
[15] S. Picciotto, M.E. Barone, D. Fierli, A. Aranyos, G. Adamo, D. Božič, D. P. Romancino, C. Stanly, R. Parkes, S. Morsbach, S. Raccosta, C. Paganini, A. Cusimano, V. Martorana, R. Noto, R. Carrotta, F. Librizzi, U. Capasso Palmiero, P. Santonicola, A. Iglič, M. Gai, L. Corcuera, A. Kisslinger, E. Di Schiavi, K. Landfester, G.L. Liguori, V. Kralj-Iglič, P. Arosio, G. Pocsfalvi, M. Manno, N. Touzet, A. Bongiovanni, Isolation of extracellular vesicles from microalgae: towards the production of sustainable and natural nanocarriers of bioactive compounds, Biomater. Sci. 9 (2021) 2917–2930, https://doi.org/10.1039/D0BM01696A.
[16] N. Ivošević DeNardis, J. Pečar Ilić, I. Ružić, G. Pletikapić, Cell adhesion and spreading at a charged interface: insight into the mechanism using surface techniques and mathematical modelling, Electrochim. Acta 176 (2015) 743–754, https://doi.org/10.1016/j.electacta.2015.07.068.
[17] N. Ivošević DeNardis, G. Pletikapić, R. Frkanec, L. Horvat, P.T. Vernier, From algal cells to autofluorescent ghost plasma membrane vesicles, Bioelectrochemistry 134 (2020) 107524, https://doi.org/10.1016/j.bioelechem.2020.107524.
[18] M. Levak Zorinc, I. Demir-Yilmaz, C. Formosa-Dague, I. Vrana, B. Gašparović, L. Horvat, A. Butorac, R. Frkanec, N. Ivošević DeNardis, Reconstructed membrane vesicles from the microalga *Dunaliella* as a potential drug delivery system, Bioelectrochemistry 150 (2023) 108360, https://doi.org/10.1016/j.bioelechem.2022.108360.
[19] R.R.L. Guillard, Culture of phytoplankton for feeding marine invertebrates, in: W. L. Smith, M.H. Chanley (Eds.), Culture of Marine Invertebrate Animals, Springer, New York, NY, 1975, pp. 29–60.
[20] M. Lukeš, M. Giordano, O. Prášil, The effect of light quality and quantity on carbon allocation in *Chromera velia*, Folia Microbiol. 64 (2019) 655–662, https://doi.org/10.1007/s12223-019-00734-y.
[21] M. Lukeš, L. Procházková, V. Shmidt, L. Nedbalová, D. Kaftan, Temperature dependence of photosynthesis and thylakoid lipid composition in the red snow alga *Chlamydomonas* cf. *nivalis* (*Chlorophyceae*), FEMS Microbiol. Ecol. 89 (2014) 303–315, https://doi.org/10.1111/1574-6941.12299.
[22] A. Střížek, P. Přibyl, M. Lukeš, T. Grivalský, J. Kopecký, T. Galica, P. Hrouzek, *Hibberdia magna* (Chrysophyceae): a promising freshwater fucoxanthin and polyunsaturated fatty acid producer, Microb. Cell Factories 22 (2023) 73, https://doi.org/10.1186/s12934-023-02061-x.
[23] NanoScope Analysis Software, Version 2.0, Bruker, Billerica, MA, USA, 2019.
[24] JPKSPM Data Processing Software, Version 7.0.165, Bruker, Berlin, Germany, 2023.
[25] J.E. Sader, I. Larson, P. Mulvaney, L.R. White, Method for the calibration of atomic force microscope cantilevers, Rev. Sci. Instrum. 66 (1995) 3789–3798, https://doi.org/10.1063/1.1145439.
[26] N. Novosel, T. Mišić Radić, J. Zemla, M. Lekka, A. Čačković, D. Kasum, T. Legović, P. Žutinić, M. Gligora Udovič, N. Ivošević DeNardis, Temperature-induced response in algal cell surface properties and behaviour: an experimental approach, J. Appl. Phycol. 34 (2022) 243–259, https://doi.org/10.1007/s10811-021-02591-0.
[27] JPK Data Processing Software Version 8.0.103, Bruker-JPK, Germany, 2024.
[28] I.N. Sneddon, The relation between load and penetration in the axisymmetric boussines problem for a punch of arbitrary profile, Int. J. Eng. Sci. 3 (1965) 47–57, https://doi.org/10.1016/0020-7225(65)90019-4.
[29] S.V. Kontomaris, A. Stylianou, G. Chliveros, A. Malamou, AFM indentation on highly heterogeneous materials using different indenter geometries, Appl. Mech. 4 (2023) 460–475, https://doi.org/10.3390/applmech4020026.
[30] Igor Pro, Version 8.02, wave metrics, Lake Oswego, Oregon 97035, USA, 2018.
[31]].K. Mendová, M. Otáhal, M. Drab, M. Daniel, Size matters: rethinking hertz model interpretation for cell mechanics using AFM, Int. J. Mol. Sci. 25 (2024) 7186, https://doi.org/10.3390/ijms25137186.
[32] D.E. Laney, R.A. Garcia, S.M. Parsons, H.G. Hansma, Changes in the elastic properties of cholinergic synaptic vesicles as measured by atomic force microscopy, Biophys. J. 72 (1997) 806–813, https://doi.org/10.1016/S0006-3495(97)78714-9.

[33] A. Ridolfi, M. Brucale, C. Montis, L. Caselli, L. Paolini, A. Borup, A.T. Boysen, F. Loria, M.J.C. van Herwijnen, M. Kleinjan, P. Nejsum, N. Zarovni, M.H. M. Wauben, D. Berti, P. Bergese, F. Valle, AFM-based high-throughput nanomechanical screening of single extracellular vesicles, Anal. Chem. 92 (2020) 10274–10282, https://doi.org/10.1021/acs.analchem.9b05716.

[34] I. Demir, I. Lüchtefeld, C. Lemen, E. Dague, P. Guiraud, T. Zambelli, C. Formosa-Dague, Probing the interactions between air bubbles and (bio)interfaces at the nanoscale using FluidFM technology, J. Colloid Interface Sci. 604 (2021) 785–797, https://doi.org/10.1016/j.jcis.2021.07.036.

[35] N. Novosel, T. Mišić Radić, M. Levak Zorinc, J. Zemla, M. Lekka, I. Vrana, B. Gašparović, L. Horvat, D. Kasum, T. Legović, P. Žutinić, M. Gligogra Udovič, N. Ivošević DeNardis, Salinity-induced chemical, mechanical, and behavioral changes in marine microalgae, J. Appl. Phycol. 34 (2022) 1293–1309, https://doi.org/10.1007/s10811-022-02734-x.

[36] L. Habjanec, R. Frkanec, B. Halassy, J. Tomašić, Effect of liposomal formulations and immunostimulating peptidoglycan monomer (PGM) on the immune reaction to ovalbumin in mice, J. Liposome Res. 16 (2006) 1–16, https://doi.org/10.1080/08982100500528537.

[37] R. Dimova, C.M. Marques, The Giant Vesicle Book, first ed., CRC Press, Boca Raton, FL, USA, 2019.

[38] A. Vincy, S. Mazumder, Amrita, I. Banerjee, K.C. Hwang, R. Vankayala, Recent progress in red blood cells-derived particles as novel bioinspired drug delivery systems: challenges and strategies for clinical translation, Front. Chem. 10 (2022) 905256, https://doi.org/10.3389/fchem.2022.905256.

[39] G.B. Nash, H.J. Meiselman, Red cell and ghost viscoelasticity. Effects of hemoglobin concentration and in vivo aging, Biophys. J. 43 (1983) 63–73, https://doi.org/10.1016/S0006-3495(83)84324-0.

[40] M. Klacsová, K. Sebők-Nagy, T. Páli, M. Chovancová, L. Almásy, D. Uhríková, Microalgae-derived vesicles as potential carriers for therapeutic biomacromolecules, J. Drug Delivery Sci. Technol. 117 (2026) 107985, https://doi.org/10.1016/j.jddst.2026.107985.

[41] A. Katz, P. Waridel, A. Shevchenko, U. Pick, Salt-induced changes in the plasma membrane proteome of the halotolerant alga *Dunaliella salina* as revealed by blue native gel electrophoresis and nano-LC-MS/MS analysis, Mol. Cell. Proteomics 6 (2007) 1459–1472, https://doi.org/10.1074/mcp.M700002-MCP200.

[42] N. Varela, V. R., M. Angulo-Escalante, J.A. Sañudo Barajas, Production of bioethanol from biomass of microalgae *Dunaliella tertiolecta*, Int. J. Environ. Agric. Res. 2 (2016) 110–116.

[43] Z. Varga, B. Fehér, D. Kitka, A. Wacha, A. Bóta, S. Berényi, V. Pipich, J.-L. Fraikin, Size measurement of extracellular vesicles and synthetic liposomes: the impact of the hydration shell and the protein corona, Colloids Surf. B Biointerfaces 192 (2020) 111053, https://doi.org/10.1016/j.colsurfb.2020.111053.

[44] D.R. Fontana, A. Haug, Effects of sodium chloride on the plasma membrane of halotolerant *Dunaliella primolecta*: an electron spin resonance study, Arch. Microbiol. 131 (1982) 184–190, https://doi.org/10.1007/BF00405876.

[45] I. Vrana, S. Alempijević Bakija, N. Novosel, N. Ivošević DeNardis, D. Zigon, N. Ogrinc, B. Gašparović, Hyposalinity induces significant polar lipid remodeling in the marine microalga *Dunaliella tertiolecta* (Chlorophyceae), J. Appl. Phycol. 34 (2022), https://doi.org/10.1007/s10811-022-02745-8, 1457-1270.

[46] F. Pillet, E. Dague, J. Pečar Ilić, I. Ružić, M.-P. Rols, N. Ivošević DeNardis, Changes in nanomechanical properties and adhesion dynamics of algal cells during their growth, Bioelectrochemistry 127 (2019) 154–162, https://doi.org/10.1016/j.bioelechem.2019.02.011.

[47] D. Zhong, D. Zhang, T. Xie, M. Zhou, Biodegradable microalgae-based carriers for targeted delivery and imaging-guided therapy toward lung metastasis of breast cancer, Small 16 (2020) 2000819, https://doi.org/10.1002/smll.202000819.

[48] D. Zhong, D. Zhang, W. Chen, J. He, C. Ren, X. Zhang, N. Kong, W. Tao, M. Zhou, Orally deliverable strategy based on microalgal biomass for intestinal disease treatment, Sci. Adv. 7 (2021) eabi9265, https://doi.org/10.1126/sciadv.abi9265.

[49] Y. Qiao, F. Yang, T. Xie, Z. Du, D. Zhong, Y. Qi, Y. Li, W. Li, Z. Lu, J. Rao, Y. Sun, M. Zhou, Engineered algae: a novel oxygen-generating system for effective treatment of hypoxic cancer, Sci. Adv. 6 (2020) eaba5996, https://doi.org/10.1126/sciadv.aba5996.

[50] B. Atasever-Arslan, K. Yilancioglu, M.G. Bekaroglu, E. Taskin, E.A.S. Cetiner, Cytotoxic effect of extract from *Dunaliella salina* against SH-SY5Y neuroblastoma cells, Gen. Physiol. Biophys. 34 (2015) 201–207, https://doi.org/10.4149/gpb_2014034.

[51] W. Jiskoot, R.M.F. van Schie, M.G. Carstens, H. Schellekens, Immunological risk of injectable drug delivery systems, Pharm. Res. 26 (2009) 1303–1314, https://doi.org/10.1007/s11095-009-9855-9.

[52] C.T. Inglut, A.J. Sorrin, T. Kuruppu, S. Vig, J. Cicalo, H. Ahmad, H.-C. Huang, Immunological and toxicological considerations for the design of liposomes, Nanomaterials (Basel, Switzerland) 10 (2020) 190, https://doi.org/10.3390/nano10020190.

[53] V. Svetličić, A. Hozić, Probing cell surface charge by scanning electrode potential, Electrophoresis 23 (2002) 2080–2286, https://doi.org/10.1002/1522-2683(200207)23:13<2080::AID-ELPS2080>3.0.CO;2-W.

[54] L. Sercombe, T. Veerati, F. Moheimani, S.Y. Wu, A.K. Sood, S. Hua, Advances and challenges of liposome assisted drug delivery, Front. Pharmacol. 6 (2015) 286, https://doi.org/10.3389/fphar.2015.00286.

[55] D. Guimarães, A. Cavaco-Paulo, E. Nogueira, Design of liposomes as drug delivery system for therapeutic applications, Int. J. Pharm. 601 (2021) 120571, https://doi.org/10.1016/j.ijpharm.2021.120571.

[56] S. Kreimer, A.M. Belov, I. Ghiran, S.K. Murthy, D.A. Frank, A.R. Ivanov, Mass-spectrometry-based molecular characterization of extracellular vesicles: lipidomics and proteomics, J. Proteome Res. 14 (2015) 2367–2384, https://doi.org/10.1021/pr501279t.

[57] E. van der Pol, A.N. Böing, E.L. Gool, R. Nieuwland, Recent developments in the nomenclature, presence, isolation, detection and clinical impact of extracellular vesicles, J. Thromb. Haemost. 14 (2016) 48–56, https://doi.org/10.1111/jth.13190.

[58] H. Fu, Y. Chen, Q. Fu, Q. Lv, J. Zhang, T.P. Yang Yang, X. Wang, W.Z. Yang Ying, From conventional to cutting-edge: exosomes revolutionizing nano-drug delivery systems, Chem. Eng. J. 500 (2024) 156685, https://doi.org/10.1016/j.cej.2024.156685.

[59] K. Shimbo, S. Miyaki, H. Ishitobi, Y. Kato, T. Kubo, S. Shimose, M. Ochi, Exosome-formed synthetic microRNA-143 is transferred to osteosarcoma cells and inhibits their migration, Biochem. Biophys. Res. Commun. 445 (2014) 381–387, https://doi.org/10.1016/j.bbrc.2014.02.007.

[60] Z.Q. Yuan, K.K. Kolluri, K.H.C. Gowers, S.M. Janes, TRAIL delivery by MSC-derived extracellular vesicles is an effective anticancer therapy, J. Extracell. Vesicles 6 (2017) 1265291, https://doi.org/10.1080/20013078.2017.1265291.

[61] L. Pascucci, V. Coccè, A. Bonomi, D. Ami, P. Ceccarelli, E. Ciusani, L. Viganò, A. Locatelli, F. Sisto, S.M. Doglia, E. Parati, M.E. Bernardo, M. Muraca, G. Alessandri, G. Bondiolotti, A. Pessina, Paclitaxel is incorporated by mesenchymal stromal cells and released in exosomes that inhibit in vitro tumor growth: a new approach for drug delivery, J. Control. Release 192 (2014) 262–270, https://doi.org/10.1016/j.jconrel.2014.07.042.

[62] V. Yarlagadda, S. Samaddar, K. Paramanandham, B.R. Shome, J. Haldar, Membrane disruption and enhanced inhibition of cell-wall biosynthesis: a synergistic approach to tackle vancomycin-resistant bacteria, Angew. Chem. 127 (2015) 13848–13853, https://doi.org/10.1002/ange.201507567.

[63] T. Studer, D. Morina, I.S. Shchelik, K. Gademann, Biohybrid microswimmers for antibiotic drug delivery based on a thiol-sensitive release platform, Chemistry (Weinheim an der Bergstrasse, Germany) 29 (2023) e202203913, https://doi.org/10.1002/chem.202203913.